#### RESEARCH ARTICLE



Check for updates

# Solid state synthesis of BiFeO<sub>3</sub> occurs through the intermediate Bi<sub>25</sub>FeO<sub>39</sub> compound

## Correspondence

Corrado Wesley and Jacob L. Jones, Department of Materials Science, North Carolina State University, Raleigh, NC 27695, USA.

Email: corradojh@gmail.com and jljone21@ncsu.edu

#### Funding information

Center for Dielectrics and Piezoelectrics, North Carolina State University, Grant/Award Numbers: ECCS-2025064, IIP-1841453, IIP-1841466

#### **Abstract**

The solid-state synthesis of perovskite BiFeO<sub>3</sub> has been a topic of interest for decades. Many studies have reported challenges in the synthesis of BiFeO<sub>3</sub> from starting oxides of Bi<sub>2</sub>O<sub>3</sub> and Fe<sub>2</sub>O<sub>3</sub>, mainly associated with the development of persistent secondary phases such as Bi<sub>25</sub>FeO<sub>39</sub> (sillenite) and Bi<sub>2</sub>Fe<sub>4</sub>O<sub>9</sub> (mullite). These secondary phases are thought to be a consequence of unreacted Fe-rich and Bi-rich regions, that is, incomplete interdiffusion. In the present work, in situ high-temperature X-ray diffraction is used to demonstrate that Bi<sub>2</sub>O<sub>3</sub> first reacts with Fe<sub>2</sub>O<sub>3</sub> to form sillenite Bi<sub>25</sub>FeO<sub>39</sub>, which then reacts with the remaining Fe<sub>2</sub>O<sub>3</sub> to form BiFeO<sub>3</sub>. Therefore, the synthesis of perovskite BiFeO<sub>3</sub> is shown to occur via a two-step reaction sequence with Bi<sub>25</sub>FeO<sub>39</sub> as an intermediate compound. Because  $Bi_{25}FeO_{39}$  and the  $\gamma$ - $Bi_2O_3$  phase are isostructural, it is difficult to discriminate them solely from X-ray diffraction. Evidence is presented for the existence of the intermediate sillenite Bi<sub>25</sub>FeO<sub>39</sub> using quenching experiments, comparisons between Bi<sub>2</sub>O<sub>3</sub> behavior by itself and in the presence of Fe<sub>2</sub>O<sub>3</sub>, and crystal structure examination. With this new information, a proposed reaction pathway from the starting oxides to the product is presented.

#### KEYWORDS

ferrites, ferroelectricity/ferroelectric materials, perovskites, synthesis, X-ray methods

## 1 | INTRODUCTION

BiFeO<sub>3</sub> is a scientifically and industrially interesting ferroic oxide because it can exhibit both antiferromagnetic and ferroelectric properties. The synthesis of BiFeO<sub>3</sub> is typically undertaken by solid-state reaction of the starting oxides of  $Bi_2O_3$  and  $Fe_2O_3$  in the region of 750°C, although techniques such as wet chemical and sol–gel methods have been explored with some success.<sup>2,3</sup> Although the

solid-state reaction of  $BiFeO_3$  from  $Bi_2O_3$  and  $Fe_2O_3$  is simple in chemical formula, significant complications and challenges have been reported.

A description of solid-state synthesis was outlined by Bernardo et al.  $^4$  in which it was proposed that the Bi $_2$ O $_3$  diffuses into the Fe $_2$ O $_3$  particle, which then forms BiFeO $_3$ . This schematic diagram is reproduced in Figure 1. In Figure 1, the idealized final stage of the reaction is shown with the arrow toward the top-right of the figure, a process

This is an open access article under the terms of the Creative Commons Attribution License, which permits use, distribution and reproduction in any medium, provided the original work is properly cited.

© 2024 The Authors. Journal of the American Ceramic Society published by Wiley Periodicals LLC on behalf of American Ceramic Society.

<sup>&</sup>lt;sup>1</sup>Department of Materials Science and Engineering, North Carolina State University, Raleigh, North Carolina, USA

<sup>&</sup>lt;sup>2</sup>Analytical Instrumentation Facility, North Carolina State University, Raleigh, North Carolina, USA

<sup>&</sup>lt;sup>3</sup>Department of Materials Science and Engineering, Carnegie Mellon University, Pittsburgh, Pennsylvania, USA

<sup>&</sup>lt;sup>4</sup>Department of Materials Science and Engineering, University of Sheffield, Sheffield, UK

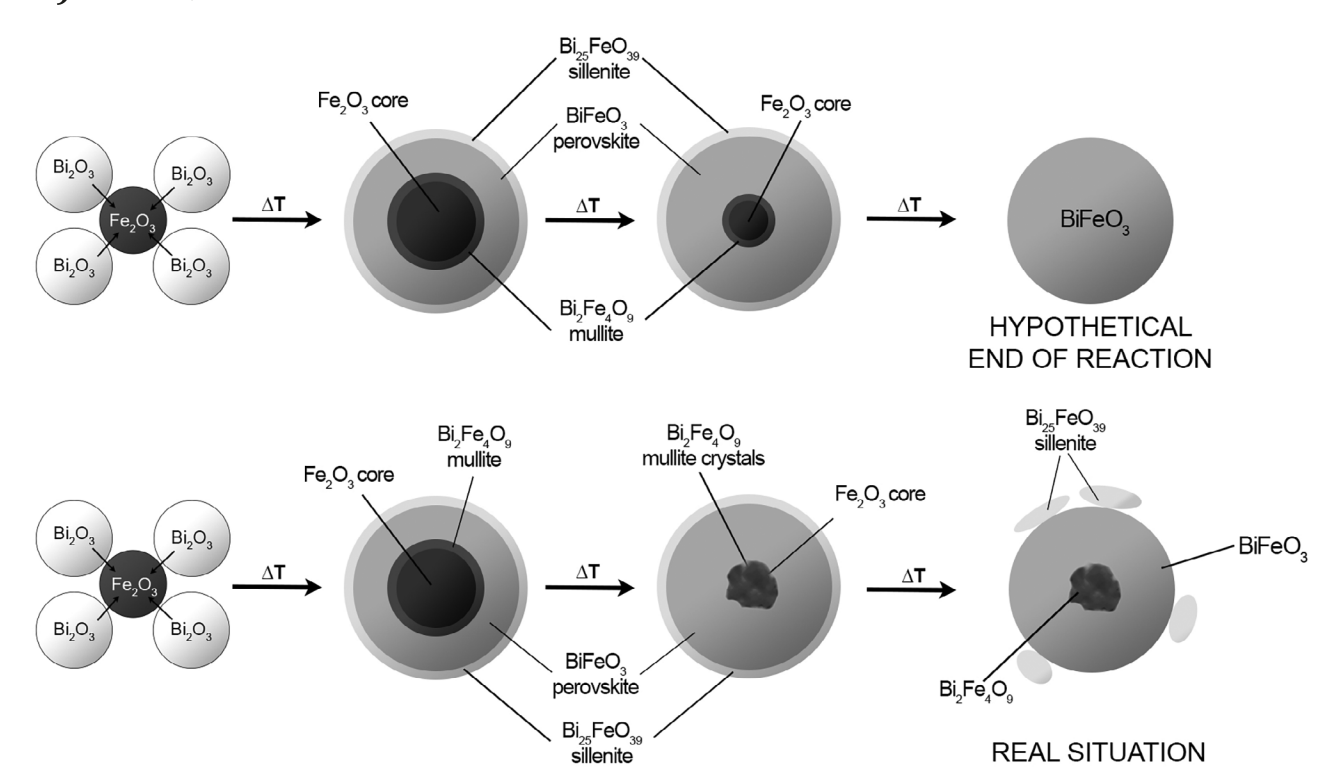


FIGURE 1 The reaction pathway for Bi<sub>2</sub>O<sub>3</sub>-Fe<sub>2</sub>O<sub>3</sub> to BiFeO<sub>3</sub> redrawn after and adapted from Bernardo et al.<sup>4</sup>

resulting in homogeneous  $BiFeO_3$ . However, interdiffusion is required between  $Bi_2O_3$  and  $Fe_2O_3$ , which allows other, undesirable compounds to form, and the chemical gradient can result in a core-shell structure. With diffusion of  $Bi_2O_3$  into the  $Fe_2O_3$  particle, the initial core of  $Fe_2O_3$  evolves to an iron-rich  $Bi_2Fe_4O_9$  (mullite) phase, which is a line compound, leaving the shell Fe-deficient. Some  $BiFeO_3$  develops, with remaining Bi-rich material forming  $Bi_{25}FeO_{39}$  (sillenite) phase, another line compound.  $Bi^{3+}$  and  $Fe^{3+}$  from the precursor are trapped within these secondary phases, inhibiting further reaction to form the perovskite phase.

It is also important to note that BiFeO<sub>3</sub> is a line compound itself. A phase diagram is given in Palai et al.<sup>5</sup> showing that if the composition deviates from this line, then secondary phases such as sillenite and mullite become favorable. Valant et al.<sup>6</sup> further emphasized that these secondary phases are thermodynamically favorable and are further stabilized by the presence of impurities.

While  $Fe_2O_3$  is not expected to exhibit polymorphic phase transitions within the formation temperature of  $BiFeO_3$ ,  $Bi_2O_3$  is monoclinic (designated  $\alpha$ - $Bi_2O_3$ ) at room temperature and undergoes polymorphic phase transitions on heating,<sup>5</sup> which possibly influences the reaction. Reported phases in  $Bi_2O_3$  include monoclinic  $\alpha$ - $Bi_2O_3$ , face-centered cubic (fcc)  $\delta$ - $Bi_2O_3$  (the high temperature cubic phase), and body-centered cubic (bcc)  $\gamma$ - $Bi_2O_3$  (a metastable cubic phase).<sup>5</sup> However, there is no consensus

on the phase transitions occurring during the reaction to form BiFeO<sub>3</sub> and their role in the synthesis itself. Morozov et al. Paper that the  $\alpha$ -Bi<sub>2</sub>O<sub>3</sub> phase converts to the  $\gamma$ -Bi<sub>2</sub>O<sub>3</sub> at approximately 730°C. Thrall et al. using in situ high-temperature X-ray diffraction (HTXRD), reported that  $\alpha$ -Bi<sub>2</sub>O<sub>3</sub> converts to  $\gamma$ -Bi<sub>2</sub>O<sub>3</sub> at approximately 650–700°C under vacuum and inert environments. However, previous reports suggest that  $\alpha$ -Bi<sub>2</sub>O<sub>3</sub> converts to  $\delta$ -Bi<sub>2</sub>O<sub>3</sub> at 730°C, and that  $\gamma$ -Bi<sub>2</sub>O<sub>3</sub> is only observed during cooling from the higher temperature  $\delta$ -Bi<sub>2</sub>O<sub>3</sub> phase. Pall

There is evidence in the literature that between 447 and 767°C, BiFeO<sub>3</sub> is metastable, and decomposes into thermodynamically stable secondary phases, often with remaining starting oxides present.<sup>1</sup> A study by Selbach et al.<sup>12</sup> showed that BiFeO<sub>3</sub> decomposed to secondary phases between 600 and 900°C, and then re-formed BiFeO<sub>3</sub> at higher temperatures. Morozov et al.<sup>7</sup> claimed that BiFeO<sub>3</sub> always yields other compounds as impurities. These results evidence the challenges of synthesizing pure-phase BiFeO<sub>3</sub> using solid-state reactions.

Understanding the reaction fully requires the in situ identification of phases, which is most appropriate for X-ray diffraction (XRD). However, a central challenge in following the phase evolution during the synthesis of BiFeO<sub>3</sub> using XRD is that metastable  $\gamma$ -Bi<sub>2</sub>O<sub>3</sub> is isostructural to Bi<sub>25</sub>FeO<sub>39</sub><sup>13,14</sup>; consequently, the XRD patterns of the two phases are difficult to distinguish from one another. However, there exist various approaches for

journal<sub>⊥³</sub>

discerning the phases. One approach is to closely examine the cell metrics. For example, Levin and Roth <sup>15</sup> reported that the lattice parameters of an undoped, metastable bcc phase of Bi $_2$ O $_3$  are much larger than a distinct, stable bcc phase of Bi $_2$ O $_3$  with Fe $_2$ O $_3$  incorporation. Figure S1 <sup>15</sup> in Supporting Information shows the expected lattice parameters. Of relevance to the current work is the undoped, metastable bcc phase of Bi $_2$ O $_3$  lattice parameter of 10.27 Å, and the distinct, stable bcc phase of approximately 4 mol% Fe $_2$ O $_3$ -modified Bi $_2$ O $_3$ , which is approximately 10.19 Å. These lattice parameters are referenced further in the following sections.

To provide insight into the solid-state reaction of  $Bi_2O_3$  and  $Fe_2O_3$  to form  $BiFeO_3$ , several in situ HTXRD experiments are presented. In situ HTXRD experiments include heating and cooling the starting oxides individually at multiple heating rates in air, heating and cooling mixed starting oxides to form  $BiFeO_3$ , and partially heating mixed starting oxides that were quenched. These experiments demonstrate that all the  $Bi_2O_3$  reacts with a small amount of  $Fe_2O_3$  to form sillenite  $Bi_{25}FeO_{39}$  prior to the formation of  $BiFeO_3$ . In other words, the reaction of  $Bi_2O_3$  with  $Fe_2O_3$  to form  $BiFeO_3$  occurs via a two-step reaction sequence with sillenite  $Bi_{25}FeO_{39}$  as the intermediate compound.

## 2 | EXPERIMENTAL PROCEDURES

Starting powders of Bi<sub>2</sub>O<sub>3</sub> (99.99%, Alfa Aesar) and Fe<sub>2</sub>O<sub>3</sub> (99.99%, Alfa Aesar) were weighed in equimolar proportions to target the formation of BiFeO<sub>3</sub>. All experiments involved ball milling of the powders prior to HTXRD in ethanol for 24 h using 10 mm yttria stabilized zirconia milling media (20:1). No milling media contamination was observed in the products after the milling process. A scanning electron microscope (SEM) image of the milled powder is provided in Figure S2 and shows that the Bi<sub>2</sub>O<sub>3</sub> and Fe<sub>2</sub>O<sub>3</sub> particles are on the scale of approximately 1  $\mu$ m and 100 nm, respectively. All powders were heated in an Anton Paar XRK 900 reaction chamber with z-stage automated alignment while mounted in a PANalytical Empyrean powder diffractometer with Cu K $\alpha$  radiation under an ambient gas with a heating rate of 1°C/min. In situ HTXRD patterns were measured continuously in a  $2\theta$  range of  $20^{\circ}$ – $80^{\circ}$  using a step size of 0.026°. In situ patterns were also measured during cooling at a rate of 10°C/min.

## 3 | RESULTS AND DISCUSSION

An important aspect of this work is to identify the role of the phase transitions in Bi<sub>2</sub>O<sub>3</sub> in the synthesis of BiFeO<sub>3</sub>.

It is therefore critical to differentiate between the isostructural phases of  $\gamma$ -Bi<sub>2</sub>O<sub>3</sub> and Bi<sub>25</sub>FeO<sub>39</sub>. With that in mind, the phase transitions in Bi<sub>2</sub>O<sub>3</sub> when heated by itself to 780°C at 1°C/min, held at that temperature for 1 h, then cooled at 10°C/min to room temperature are determined and these results are presented in Figure 2A. Figure S3 shows these results over a wider  $2\theta$  range. Fe<sub>2</sub>O<sub>3</sub> was heat treated under the same conditions, though there were no phase transitions observed (results not shown here).

The in situ HTXRD scan in Figures 2A and S3 shows that when  $\alpha$ -Bi<sub>2</sub>O<sub>3</sub> is heated by itself, the initial monoclinic α-Bi<sub>2</sub>O<sub>3</sub> persists to between 700 and 750°C, at which temperature it transitions to fcc  $\delta$ -Bi<sub>2</sub>O<sub>3</sub>. On cooling, the  $\delta$ -Bi<sub>2</sub>O<sub>3</sub> converts to  $\gamma$ -Bi<sub>2</sub>O<sub>3</sub>, which is consistent with Harwig and Gerards<sup>11</sup> and Levin and Roth.<sup>15</sup> In the present study as well as in the works of Harwig and Gerards<sup>11</sup> and Levin and Roth,  $^{16}$  the  $\gamma$ -Bi<sub>2</sub>O<sub>3</sub> phase is only observed during cooling. At approximately 500°C during cooling, the  $\gamma$ -Bi<sub>2</sub>O<sub>3</sub> transitions to  $\alpha$ -Bi<sub>2</sub>O<sub>3</sub>, demonstrating reversibility to the original phase upon cooling. In other experiments not shown here, milled  $\alpha$ -Bi<sub>2</sub>O<sub>3</sub> powders were heated at 1°C/min and unmilled  $\alpha$ -Bi<sub>2</sub>O<sub>3</sub> was heated at 5°C/min, and the same phase transitions were observed, showing the persistence of this observation with different sample preparation methods and heating rates. The observation that  $\gamma$ -Bi<sub>2</sub>O<sub>3</sub> is not present on heating is discussed later in the manuscript in relation to the reactions to form BiFeO<sub>3</sub>.

To synthesize BiFeO<sub>3</sub>, an equimolar mixture of milled  $Bi_2O_3$  and  $Fe_2O_3$  was heated to  $780^{\circ}C$ , a temperature, determined from iterative experiments, which enabled full reaction to form BiFeO<sub>3</sub>. The HTXRD measurements of the full reaction to form BiFeO<sub>3</sub> are shown in Figure 2B. Figure S4 shows these results over a wider  $2\theta$  range.

There are several features to highlight in the in situ HTXRD measurements in Figures 2B and S4. First, all the  $\alpha$ -Bi<sub>2</sub>O<sub>3</sub> converts into a different crystal structure at approximately 600°C. In Figure 2A,  $\alpha$ -Bi<sub>2</sub>O<sub>3</sub> by itself does not appear to change phase until approximately 750°C, at which temperature it converts to  $\delta$ -Bi<sub>2</sub>O<sub>3</sub>. The comparison of this initial observation (in Figure 2B) to that of Bi<sub>2</sub>O<sub>3</sub> heated by itself (Figure 2A) indicates a possible phase transition and/or an intermediate phase. More specifically, that Fe causes this intermediate phase, suggests that it is likely sillenite,  $Bi_{25}FeO_{39}$ , rather than  $\gamma$ - $Bi_2O_3$ . Another important observation in Figure 2B is that BiFeO<sub>3</sub> starts to form at approximately 700°C, before the Bi<sub>25</sub>FeO<sub>39</sub> phase has completely disappeared. As the sillenite phase disappears, mullite forms and persists through the entire thermal process. The mullite phase peak positions agree with positions reported previously in literature.1 With continued heating, the remainder of the Fe<sub>2</sub>O<sub>3</sub> reacts with the sillenite to form BiFeO<sub>3</sub>. On cooling (Figure 2B), the BiFeO<sub>3</sub> product remains.

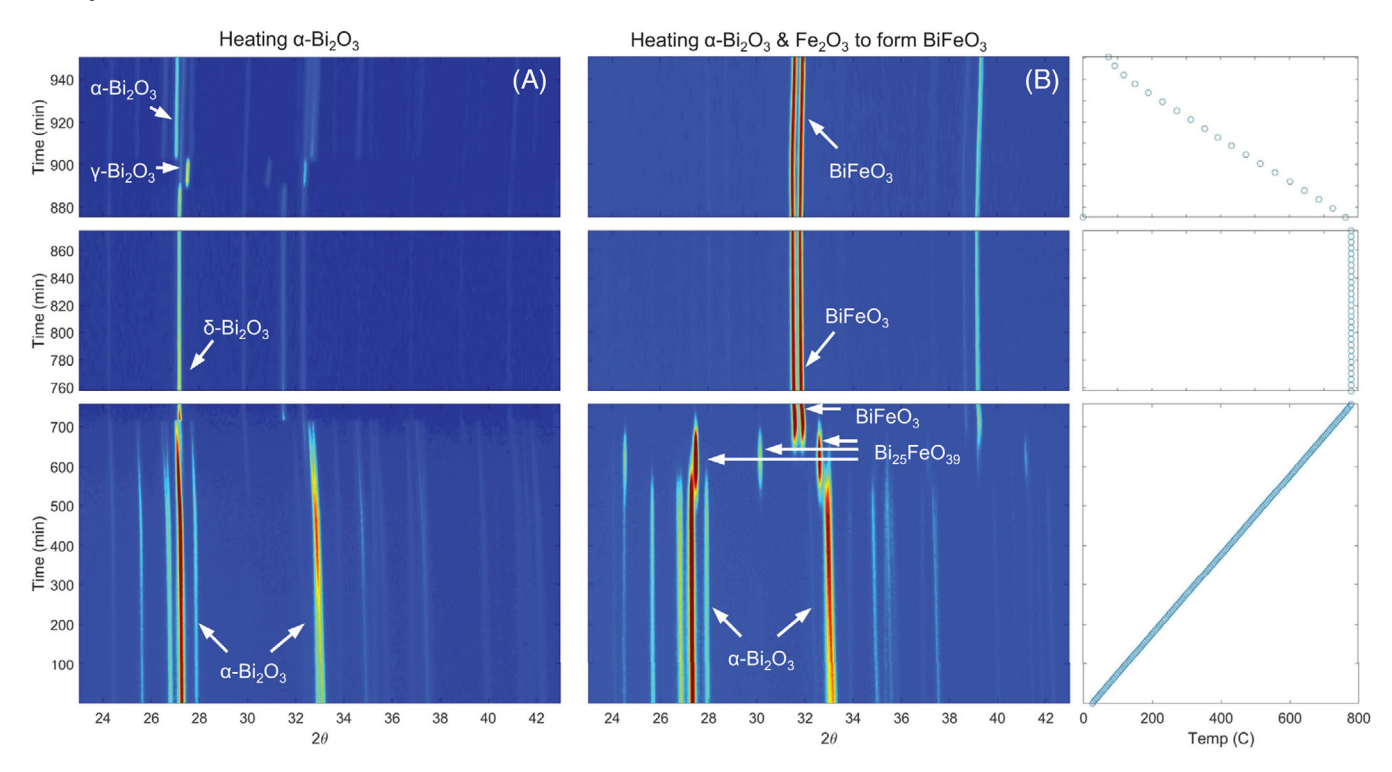


FIGURE 2 Powder diffraction patterns measured in situ during high-temperature X-ray diffraction (HTXRD) of (A) Bi<sub>2</sub>O<sub>3</sub> heating and cooling by itself, and (B) Bi<sub>2</sub>O<sub>3</sub> and Fe<sub>2</sub>O<sub>3</sub> heated to react and form BiFeO<sub>3</sub>.

In the specific experiment shown in Figure 2B, the persistence of a very minor fraction of  $\mathrm{Bi}_2\mathrm{Fe}_4\mathrm{O}_9$  is a reminder of the importance of starting particle size, as can be inferred from Figure 1. By repeating this experiment multiple times, examples can be found where the final products are phase-pure  $\mathrm{BiFeO}_3$  within the resolution limits of diffraction. The variability in the final phase is a consequence of the small quantities of powders used in the HTXRD experiment and their state of mixing when placed on the heating stage. An indexed pattern of a resulting phase-pure  $\mathrm{BiFeO}_3$  in one of these experiments is shown in Figure 3.

Another important observation that needs to be informed for understanding of the reaction sequence is the behavior of the Fe<sub>2</sub>O<sub>3</sub> diffraction peaks. The intensity of Bi<sub>2</sub>O<sub>3</sub> is much higher than that of Fe<sub>2</sub>O<sub>3</sub> (mostly attributed to the difference in atomic scattering factors of Bi vs. Fe), meaning that most of the reflections in the lower  $2\theta$  region of Figure 2B are assigned to Bi<sub>2</sub>O<sub>3</sub>. The major peaks of the initial rhombohedral Fe<sub>2</sub>O<sub>3</sub> phase (PDF pattern 04-015-6947) are at  $2\theta$  approximately 24.15° (012 reflection), and at  $2\theta$  approximately 33.16° (104 reflection), which lies in the same  $2\theta$  range as  $\alpha$ -Bi<sub>2</sub>O<sub>3</sub> 122/200. To illustrate the reaction sequence more closely, a magnified section of Figure 2B is included as shown in Figure 4.

Figure 4 shows that the  $\alpha$ -Bi<sub>2</sub>O<sub>3</sub> (peak at approximately 21.7° 2 $\theta$ ) disappears by approximately 545°C, much lower than the beginning of BiFeO<sub>3</sub> formation. The disappear-

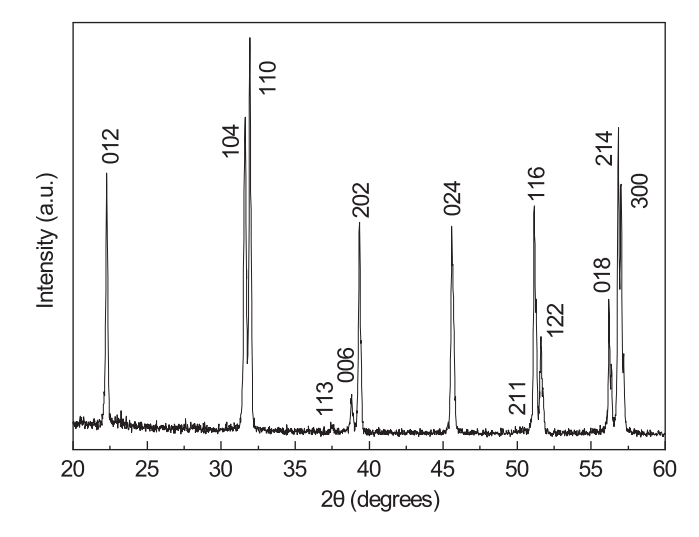
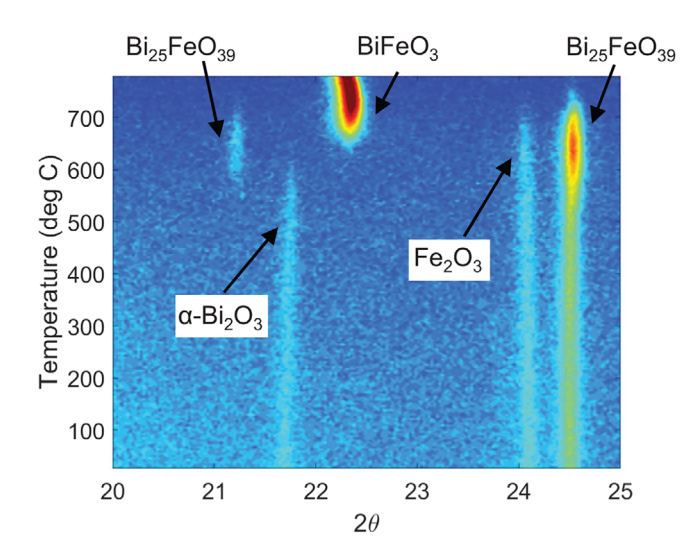


FIGURE 3 Indexed diffraction pattern of BiFeO<sub>3</sub> resulting from a high-temperature X-ray diffraction (HTXRD) experiment.

ance of the  $\alpha$ -Bi<sub>2</sub>O<sub>3</sub> peak does, however, coincide with the appearance of the peak at approximately 21.1°  $2\theta$  (which could be assigned to either Bi<sub>25</sub>FeO<sub>39</sub> or  $\gamma$ -Bi<sub>2</sub>O<sub>3</sub>). The Fe<sub>2</sub>O<sub>3</sub> (peak at approximately 21.1°  $2\theta$ ) persists to at least 100°C higher than the  $\alpha$ -Bi<sub>2</sub>O<sub>3</sub>. The peak at approximately 24.5°  $2\theta$  is initially  $\alpha$ -Bi<sub>2</sub>O<sub>3</sub>, and then intensifies, which appears to be a major peak of the intermediate phase. The persistence of the peak at approximately 24.5°  $2\theta$  suggests a crystallographic relationship between the  $\alpha$ -Bi<sub>2</sub>O<sub>3</sub> and the intermediate phase (Bi<sub>25</sub>FeO<sub>39</sub> or  $\gamma$ -Bi<sub>2</sub>O<sub>3</sub>).



**FIGURE 4** Magnified view of Figure 2 in the  $2\theta$  range of  $20^{\circ}$ – $25^{\circ}$ C.

To further study the intermediate phase, a separate in situ reaction was performed and quenched with the aim of locking in the intermediate phase (Bi $_{25}$ FeO $_{39}$  or  $\gamma\text{-Bi}_2O_3$ ), for example, to examine (ir)reversibility of the phase transitions. The experiment involved heating equimolar Bi $_2O_3$  and Fe $_2O_3$  at a 1°C/min heating rate to 650°C, then cooled at 20°C/min to room temperature. The result of this experiment is shown in Figure 5A. Multiple room temperature XRD patterns are recorded over several days following the experiment and a representative pattern is shown in Figure 5B.

Figure 5A shows that the intermediate phase appears at the times and temperatures expected relative to that shown earlier in Figure 2B. After quenching from 650°C to room temperature, the intermediate phase persists, as shown in Figure 5B. Referring to the experiment involving heating of Bi<sub>2</sub>O<sub>3</sub> by itself (Figure 2A), if the intermediate phase is metastable  $\gamma$ -Bi<sub>2</sub>O<sub>3</sub>, it should revert to  $\alpha$ -Bi<sub>2</sub>O<sub>3</sub> on cooling. However, the room temperature XRD patterns after quenching (e.g., Figure 5B) show the persistence of sillenite Bi<sub>25</sub>FeO<sub>39</sub> for several days after the experiment. The phases present at room temperature after the interrupted reaction are Bi<sub>25</sub>FeO<sub>39</sub>, Fe<sub>2</sub>O<sub>3</sub>, and a minor fraction of BiFeO<sub>3</sub>. Most importantly, no  $\alpha$ -Bi<sub>2</sub>O<sub>3</sub> remains after cooling. The persistence of the intermediate phase after cooling proves that it is not  $\gamma$ -Bi<sub>2</sub>O<sub>3</sub> and is consistent with the formation of Bi<sub>25</sub>FeO<sub>39</sub>.

The quenched powders are also investigated using transmission electron microscopy with energy-dispersive spectroscopy (EDS) and representative images are shown in Figure 6. The EDS maps show two distinct regions which are consistent with the XRD observations: (i) regions "1" are from the larger of two particle sizes which are

Bi-rich with a small amount of Fe distributed homogeneously throughout, consistent with the sillenite phase, and (ii) regions "2" are from the smaller particle size which are Fe-rich with no Bi, consistent with Fe<sub>2</sub>O<sub>3</sub>. These two types of particles are commensurate with the results from XRD, which shows a mixture of  $Bi_{25}FeO_{39}$  and  $Fe_2O_3$ .

Since Figure 6 illustrates that Fe has diffused homogeneously throughout the particles that were originally Bi<sub>2</sub>O<sub>3</sub>, it is natural to question whether larger particles of Bi<sub>2</sub>O<sub>3</sub> would still react with the Fe<sub>2</sub>O<sub>3</sub> to form sillenite, given that they require longer diffusion lengths. To test whether sillenite forms when starting with larger particles, Bi<sub>2</sub>O<sub>3</sub> was intentionally coarsened to increase the grain size, using a heating rate of 1°C/min, a hold at 650°C for 2 h, and then cooling at a rate of 5°C/min. The coarsened Bi<sub>2</sub>O<sub>3</sub> particles were then combined with equimolar Fe<sub>2</sub>O<sub>3</sub> and heated in the diffractometer. The HTXRD results, reported in Figure S5, show that the sillenite phase occurs in parallel to the disappearance of the Bi<sub>2</sub>O<sub>3</sub> phase. With further heating, the sillenite reacts with Fe<sub>2</sub>O<sub>3</sub> to form BiFeO<sub>3</sub>, and some sillenite phase is retained in the final pattern. Fe can, therefore, still diffuse into larger Bi<sub>2</sub>O<sub>3</sub> particles, forming sillenite during the reaction. SEM images and EDS maps of the starting particles and the final products of this experiment are shown in Figure S6. The SEM images and EDS maps are consistent with the HTXRD results, showing that some BiFeO3 forms while the larger particles exacerbate the persistence of the sillenite phase.

Data from the XRD pattern shown in Figure 5B are used to refine crystal structure models using the Rietveld method. The XRD pattern was modeled using either the  $Bi_{25}FeO_{39}$  phase or the  $\gamma$ - $Bi_2O_3$  phase. Although the final phase is already proven through the quenching study to not be  $\gamma$ -Bi<sub>2</sub>O<sub>3</sub>, we nevertheless model this phase to compare to the work of Levin and Roth.<sup>15</sup> Both calculated patterns fitted the experimental pattern well, with Bragg R factors of approximately 4%. The refinement using Bi<sub>25</sub>FeO<sub>39</sub> resulted in marginally better fit parameters, however it was not sufficiently better that it could be used as a basis for determining which phase is present, demonstrating the need for complementary experiments, such as heating of the powders independently (e.g., Figure 2A). Figure S7 shows the results of this refinement when using Bi<sub>25</sub>FeO<sub>39</sub> as the major phase which was used to obtain the cubic unit cell parameter. The refined lattice parameter is 10.1876(3) Å which matches the distinct, stable bcc phase of Bi<sub>2</sub>O<sub>3</sub> with Fe<sub>2</sub>O<sub>3</sub> incorporation ( $\sim$ 10.18 Å) in Figure S1, <sup>15</sup> better than Bi<sub>2</sub>O<sub>3</sub> ( $\sim$ 10.27 Å), supporting the presence of the intermediate phase, Bi<sub>25</sub>FeO<sub>39</sub>.

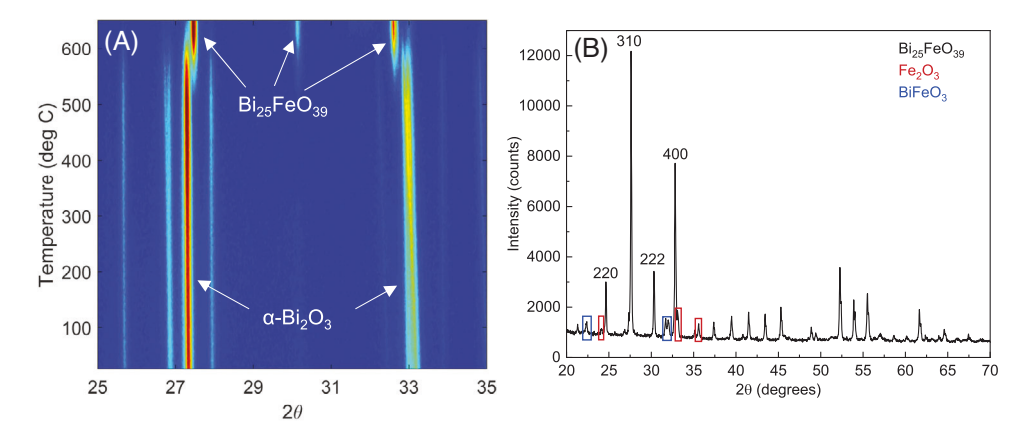


FIGURE 5 (A) Powder diffraction patterns measured in situ during high-temperature X-ray diffraction (HTXRD) of  $Bi_2O_3$  with  $Fe_2O_3$  up to 650°C, after which the sample was furnace-quenched. (B) Room temperature X-ray diffraction (XRD) pattern of the quenched product, showing the major phase of  $Bi_2SFeO_3$ , with minor amounts of  $Fe_2O_3$  (unreacted starting material), and the first appearance of product  $BiFeO_3$ .

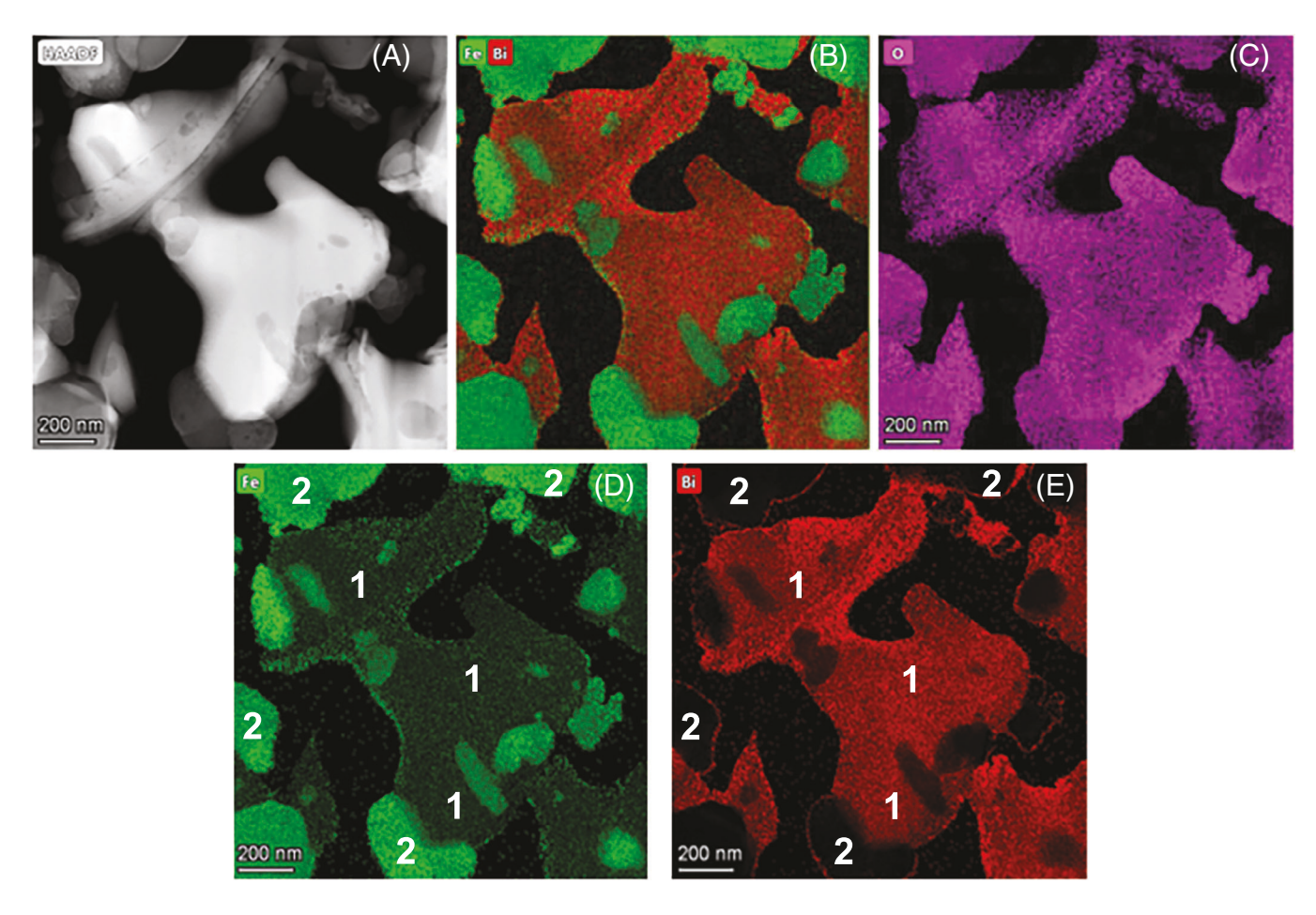


FIGURE 6 Transmission electron microscopy (TEM) image and energy-dispersive spectroscopy (EDS) maps of the equimolar  $Bi_2O_3$  and  $Fe_2O_3$  mixture that was heated to 650°C and then quenched in order to examine the intermediate phase. High-angle annular dark field (HAADF) in (A), combined Fe and Bi chemical map in (B), O map in (C), Fe map in (D), and Bi map in (E). In parts (D) and (E), two types of particles are identified, 1 and 2, which correspond to the sillenite phase and remaining  $Fe_2O_3$ , respectively.

FIGURE 7 Schematic diagram illustrating the reaction sequence of Bi<sub>2</sub>O<sub>3</sub> and Fe<sub>2</sub>O<sub>3</sub> during the formation of BiFeO<sub>3</sub>.

## 4 | CONCLUSIONS

Collectively, these experiments demonstrate that the reaction of Bi<sub>2</sub>O<sub>3</sub> with Fe<sub>2</sub>O<sub>3</sub> to form BiFeO<sub>3</sub> occurs through an intermediate phase; specifically, the Bi<sub>2</sub>O<sub>3</sub> transforms to Bi<sub>25</sub>FeO<sub>39</sub> through the incorporation of a small fraction of the Fe<sub>2</sub>O<sub>3</sub>. It is emphasized that all the Bi<sub>2</sub>O<sub>3</sub> transforms to Bi<sub>25</sub>FeO<sub>39</sub>. Thus, Bi<sub>25</sub>FeO<sub>39</sub> is not only present due to the chemical gradients innate to Bi<sub>2</sub>O<sub>3</sub> and Fe<sub>2</sub>O<sub>3</sub> interdiffusion<sup>4</sup> and from thermodynamic decomposition from BiFeO<sub>3</sub>;<sup>1,13</sup> in addition, Bi<sub>25</sub>FeO<sub>39</sub> forms as an intermediate compound in the reaction that further reacts with remaining Fe<sub>2</sub>O<sub>3</sub> to form BiFeO<sub>3</sub>. The reaction sequence in the solid-state synthesis of BiFeO3 is illustrated in Figure 7. Sillenite Bi<sub>25</sub>FeO<sub>39</sub> is indicated as an intermediate phase that reacts with the remainder of the Fe<sub>2</sub>O<sub>3</sub> to yield BiFeO<sub>3</sub>. Given these new insights that Bi<sub>25</sub>FeO<sub>39</sub> is inevitably formed during the synthesis of BiFeO<sub>3</sub>, continuing studies can focus on other factors such as the purity of the starting materials, the Bi:Fe stoichiometry, and the particle sizes.

In summary, the experiments demonstrate that sillenite  $Bi_{25}FeO_{39}$  occurs as an intermediate product of  $Bi_2O_3$  and a small amount of  $Fe_2O_3$ . All the  $Bi_2O_3$  reacts to form sillenite  $Bi_{25}FeO_{39}$ , which then reacts with the remaining  $Fe_2O_3$  to form the product  $BiFeO_3$ . Therefore, the synthesis of perovskite  $BiFeO_3$  is shown to occur via a two-step reaction sequence with  $Bi_{25}FeO_{39}$  as an intermediate compound.

## **ACKNOWLEDGMENTS**

This work was supported by the National Science Foundation (NSF), as part of the Center for Dielectrics and Piezoelectrics under grant nos. IIP-1841453 and IIP-1841466. This work was performed at the Analytical Instrumentation Facility (AIF) at North Carolina State University and at the NC State Nanofabrication Facility (NNF), both of which are supported by the State of North Carolina

and the National Science Foundation (Award No. ECCS-2025064). AIF and NNF are members of the North Carolina Research Triangle Nanotechnology Network (RTNN), a site in the National Nanotechnology Coordinated Infrastructure (NNCI). Dr. Alexandra Goodnight is acknowledged for redrawing Figure 1 and creating Figure 7, Darrell Harry for assistance with the SEM experiments, and Dr. Chris Winkler for assistance with the TEM experiments.

### ORCID

Corrado Wesley https://orcid.org/0000-0001-6964-7265 Elizabeth C. Dickey https://orcid.org/0000-0003-4005-7872

*Jacob L. Jones* https://orcid.org/0000-0002-9182-0957

#### REFERENCES

- Rojac T, Bencan A, Malic B, Tutuncu G, Jones JL, Daniels JE, et al. BiFeO<sub>3</sub> ceramics: processing, electrical, and electromechanical properties. J Am Ceram Soc. 2014;97(7):1993– 2011.
- Selbach SM, Einarsrud M-A, Tybell T, Grande T. Synthesis of BiFeO<sub>3</sub> by wet chemical methods. J Am Ceram Soc. 2007;90(11):3430–34.
- 3. Xu J-H, Ke H, Jia D-C, Wang W, Zhou Y. Low-temperature synthesis of BiFeO<sub>3</sub> nanopowders via a sol-gel method. J Alloys Compd. 2009;472:473–77.
- Bernardo MS, Jardiel T, Peiteado M, Caballero AC, Villegas M. Reaction pathways in the solid state synthesis of multiferroic BiFeO<sub>3</sub>. J Eur Ceram Soc. 2011;31:3047–53.
- 5. Palai R, Katiyar RS, Schmid H, Tissot P, Clark SJ, Robertson J, et al.  $\beta$  phase and  $\gamma$ - $\beta$  metal-insulator transition in multiferroic BiFeO<sub>3</sub>. Phys Rev. 2008;B77:014110.
- Valant M, Axelsson A-K, Alford N. Peculiarities of a solid-state synthesis of multiferroic polycrystalline BiFeO<sub>3</sub>. Chem Mater. 2007;19(22):5431–36. https://doi.org/10.1021/cm071730
- Morozov MI, Lomanova NA, Gusarov V. Specific features of BiFeO<sub>3</sub> formation in a mixture of bismuth(III) and iron(III) oxides. Russ J Gen Chem. 2003;73(11):1676–80.
- 8. Thrall M, Freer R, Martin C, Azough F, Patterson B, Cernik RJ.
  An in situ study of the formation of multiferroic bismuth ferrite

- using high resolution synchrotron X-ray powder diffraction. J Eur Ceram Soc. 2008;28(13):2567–72.
- 9. Rao CNR, Subba Rao GV, S Ramdas S. Phase transformations and electrical properties of bismuth sesquioxide. J Phys Chem. 1969;73:672–75.
- 10. Hull S. Superionics: crystal structures and conduction processes. Rep Prog Phys. 2004;67:1233–314.
- 11. Harwig HA, Gerards AG. The polymorphism of bismuth sesquioxide. Thermochim Acta. 1979;28:121–31.
- Selbach SM, Einarsrud M-A, Grande T. On the thermodynamic stability of BiFeO<sub>3</sub>. Chem Mater. 2009;21:169– 173.
- 13. Salazar-Pérez AJ, Camacho-López MA, Morales-Luckie RA, Sánchez-Mendieta V, Ureña-Núñez F, Arenas-Alatorre J. Structural evolution of  ${\rm Bi_2O_3}$  prepared by thermal oxidation of bismuth nano-particles. Superf y Vacío. 2005;18(3): 4–8.
- Jebari H, Tahiri N, Boujnah M, El Bounagui O, Taibi M, Ez-Zahraouy H. Theoretical investigation of electronic, magnetic and magnetocaloric properties of Bi<sub>25</sub>FeO<sub>40</sub> compound. Phase Transit. 2021;94(3–4):147–58.

- 15. Levin EM, Roth RS. Polymorphism of bismuth sesquioxide. II. Effect of oxide additions on the polymorphism of  $\rm Bi_2O_3$ . J Res Natl Bur Stand A. 1964;68A:197–206.
- Levin EM, Roth RS. Polymorphism of bismuth sesquioxide. I. Pure Bi<sub>2</sub>O<sub>3</sub>. J Res Natl Bur Stand A. 1964;68A:189–95.

#### SUPPORTING INFORMATION

Additional supporting information can be found online in the Supporting Information section at the end of this article.

**How to cite this article:** Wesley C, Bellcase L, Forrester JS, Dickey EC, Reaney IM, Jones JL. Solid state synthesis of BiFeO<sub>3</sub> occurs through the intermediate Bi<sub>25</sub>FeO<sub>39</sub> compound. J Am Ceram Soc. 2024;1–8. https://doi.org/10.1111/jace.19702